

Orbital optical activity in noncentrosymmetric metals and superconductors

Koki Shinada* and Robert Peters

Department of Physics, Kyoto University, Kyoto 606-8502, Japan

(Dated: February 12, 2024)

We present the optical activity induced by the orbital magnetic moment in metals and superconductors using Green's function formalization. We show that an apparent singularity of the optical activity vanishes in the normal state; however, it remains finite in the superconducting state and is related to the superconducting Edelstein effect, ensuring the missing area measurement. Finally, we calculate the optical activity in a model Hamiltonian mimicking doped transition metal dichalcogenides to investigate its characteristic spectrum, and we analyze the Kerr effect to discuss a possibility to observe the optical activity in experiments.

I. INTRODUCTION

Optical activity is a ubiquitous optical phenomenon in molecular systems and solids without an inversion center [1, 2]. It originates from the nontrivial coupling between magnetism and electricity and is related to various phenomena, such as optical rotation, dichroism, and birefringence. The optical activity can be roughly divided into two phenomena: natural optical activity (NOA) and the optical magnetoelectric effect (OMEE). The NOA includes circular dichroism, which is, e.g., used to discriminate enantiomers of chiral molecules. The OMEE appears in systems without time-reversal symmetry. Since earlier observations in noncentrosymmetric molecules and solids under the magnetic field or magnetism [3–5], the OMEE has been observed in a variety of systems [6].

Optical activity is also gaining recognition for its functionality and significance in condensed matter physics. In multiferroics [7], spin order accompanying an electric polarization and chirality is spontaneously formed. The spin order generates correlations between the magnetism and the electricity, and the OMEE can be finite. In multiferroic magnets, the OMEE is also induced by spin waves, called electromagnons, and it forms a resonant peak in the THz regime [8–13]. In addition, the OMEE is used for visualizing domains of such magnets, which are often difficult to observe with conventional methods due to the absence of macroscopic magnetization [14–17].

Optical activity in solids is not as well developed as in molecular chemistry. However, various theoretical studies have been conducted in recent years. The band theory of optical activity is discussed in several works [18–27], and it has been applied to a variety of systems, including chiral crystals [28–31], twisted bilayer graphene [32–35], and topological antiferromagnets [36]. Recently, the formalization has been extended to metals [27, 34]. In addition, it is becoming clear that optical activity also plays an essential role in exotic phases, including topological materials and superconductors. For example, it is revealed that the circular dichroism in chiral multifold

semimetals is quantized and that it can be used to probe the topological nature [37–39]. Furthermore, for superconductors, it has recently been shown that the optical activity can be applied to detect the superconducting Edelstein effect, which is unique to noncentrosymmetric superconductors and has not been observed experimentally, using the missing area measurement [40]. Despite such progress regarding optical activity, research in crystals is less advanced than in molecular chemistry, and further development is required.

In this paper, we discuss the optical activity originating from orbital magnetic moments in metals and superconductors using a Green's function formalism. We discuss a no-go theorem concerning a singularity of the optical activity in Secs. II and III, and we show that the singularity appearing in the superconducting state is related to the superconducting Edelstein effect. Furthermore, we present model calculations investigating two-dimensional materials such as transition metal dichalcogenides and twisted bilayer graphene in the normal state and the superconducting state in Secs. IV and V, respectively. We also analyze the Kerr spectrum. Finally, in Sec. VI, we conclude this paper and discuss the possibility of an experimental observation.

II. ORBITAL OPTICAL ACTIVITY IN THE NORMAL STATE

In this section, we derive the orbital optical activity in the normal state using a Green's function method. The optical activity originates from the wavenumber dependence of the optical conductivity $\sigma(\mathbf{q}, \Omega)$, where \mathbf{q} and Ω are the wavenumber and the frequency of the irradiation light. $\sigma(\mathbf{q} = 0, \Omega)$ represents the uniform conductivity that changes the refractive index of a material, leading to observable effects such as the reflectance and the rotation of linearly-polarized light (Faraday rotation and Kerr rotation) in magnets. In noncentrosymmetric systems, the first-order term in the wavenumber of the optical conductivity $\partial_{\mathbf{q}}\sigma(\mathbf{q} = 0, \Omega) \cdot \mathbf{q}$ can be significant. This is the optical activity, which is the main quantity in this paper, exhibiting optical rotation, dichroism, and birefringence. It includes two parts: a spin part and an orbital part. In this paper, we only focus on the orbital part.

* shinada.koki.64w@st.kyoto-u.ac.jp

A. Green's function formalism of the orbital optical activity

We consider noninteracting systems. The Hamiltonian without an electromagnetic field is assumed to be described by the nonrelativistic quadratic kinetic energy term with a spin-orbit coupling term as

$$H_0 = \frac{\mathbf{p}^2}{2m} + V(\mathbf{x}) + \frac{1}{4m^2} \left(\frac{\partial V(\mathbf{x})}{\partial \mathbf{x}} \times \mathbf{p} \right) \cdot \boldsymbol{\sigma}. \quad (1)$$

Here, m is the electron mass, $V(\mathbf{x})$ is a periodic potential, and $\boldsymbol{\sigma}$ are the Pauli matrices representing the spin degrees of freedom. This periodic Hamiltonian is diagonalized by the Bloch theorem using the Bloch wave function $|\psi_{n\mathbf{k}}\rangle$ as $H_0 |\psi_{n\mathbf{k}}\rangle = \epsilon_{n\mathbf{k}} |\psi_{n\mathbf{k}}\rangle$, where n is the band index and \mathbf{k} is the Bloch wave number. The Bloch wave function is split into the product of a plane wave and a periodic function $|u_{n\mathbf{k}}\rangle$ as $|\psi_{n\mathbf{k}}\rangle = e^{i\mathbf{k}\cdot\mathbf{x}} |u_{n\mathbf{k}}\rangle$. We define the Bloch Hamiltonian $H_{\mathbf{k}} = e^{-i\mathbf{k}\cdot\mathbf{x}} H_0 e^{i\mathbf{k}\cdot\mathbf{x}}$, which is diagonalized by $|u_{n\mathbf{k}}\rangle$ as $H_{\mathbf{k}} |u_{n\mathbf{k}}\rangle = \epsilon_{n\mathbf{k}} |u_{n\mathbf{k}}\rangle$.

We introduce the electromagnetic field using the vector potential $\mathbf{A}(\mathbf{x}, t)$ by shifting the momentum $\mathbf{p} \rightarrow \mathbf{p} + e\mathbf{A}(\mathbf{x}, t)$ ($-e < 0$ is the electron charge). We use the temporal gauge, where the vector potential alone fully describes the electromagnetic field without a scalar potential. The vector potential yields an additional term up to the first order

$$H_A = \frac{1}{2} (\mathbf{v} \cdot \mathbf{A}(\mathbf{x}, t) + \mathbf{A}(\mathbf{x}, t) \cdot \mathbf{v}), \quad (2)$$

where $\mathbf{v} = i[H_0, \mathbf{x}]$ is the velocity operator. Here, we ignore the diamagnetic term, which is the quadratic term, because it only contributes to the conductivity independent of \mathbf{q} and, thus, does not contribute to the optical activity. We also neglect the Zeeman term, which is the coupling between the magnetic field and the spin moment and contributes to the spin part of the optical activity [27, 40]. Focusing only on the orbital part of the optical activity in this paper, we can neglect this term.

The current operator conjugate with the vector potential $\mathbf{A}(\mathbf{r}, t)$ (\mathbf{r} is just a position coordinate, not an operator) is given by

$$\mathbf{J}(\mathbf{r}) \equiv -\frac{\delta H_A}{\delta \mathbf{A}(\mathbf{r}, t)} = -\frac{e}{2} \{\mathbf{v}, \delta(\mathbf{r} - \mathbf{x})\}. \quad (3)$$

Using the dynamical linear response theory, the current-current correlation function reads

$$\begin{aligned} & \Phi_{\mu\nu}(\mathbf{q}, \Omega) \\ &= e^2 \int [d^4k] f(\omega) \text{Tr} \left[G^{RA}(\mathbf{k}-, \omega) v_{\mathbf{k}}^\mu G^R(\mathbf{k}+, \omega + \Omega) v_{\mathbf{k}}^\nu \right. \\ & \quad \left. + G^A(\mathbf{k}-, \omega - \Omega) v_{\mathbf{k}}^\mu G^{RA}(\mathbf{k}+, \omega) v_{\mathbf{k}}^\nu \right]. \end{aligned} \quad (4)$$

Here, $G^{R/A}(\mathbf{k}, \omega) = 1/(\omega - H_{\mathbf{k}} + \mu \pm i\Gamma)$ is the retarded/advanced Green's function at a chemical potential μ , and $\mathbf{v}_{\mathbf{k}} = \partial H_{\mathbf{k}} / \partial \mathbf{k}$ is the velocity operator of the Bloch Hamiltonian. $f(\omega) = 1/(e^{\beta\omega} +$

1) is the Fermi distribution function at temperature $1/\beta$. We use the following abbreviations; $\int [d^4k] = \int_{-\infty}^{\infty} d\omega / (2\pi i) \int_{\text{BZ}} d^3k / (2\pi)^3$, $G^{RA} = G^R - G^A$, and $\mathbf{k}\pm = \mathbf{k} \pm \mathbf{q}/2$. In this paper, we phenomenologically introduce the dissipation effect by a finite Γ .

Expanding the correlation function by the wavenumber \mathbf{q} , the first-order term is given by

$$\begin{aligned} \Phi_{\mu\nu\lambda}(\Omega) &= \frac{e^2}{2} \int [d^4k] f(\omega) \\ & \quad \times \text{Tr} \left[-\partial_\lambda G^{RA}(\mathbf{k}, \omega) v_{\mathbf{k}}^\mu G^R(\mathbf{k}, \omega + \Omega) v_{\mathbf{k}}^\nu \right. \\ & \quad + G^{RA}(\mathbf{k}, \omega) v_{\mathbf{k}}^\mu \partial_\lambda G^R(\mathbf{k}, \omega + \Omega) v_{\mathbf{k}}^\nu \\ & \quad - \partial_\lambda G^A(\mathbf{k}, \omega - \Omega) v_{\mathbf{k}}^\mu G^{RA}(\mathbf{k}, \omega) v_{\mathbf{k}}^\nu \\ & \quad \left. + G^A(\mathbf{k}, \omega - \Omega) v_{\mathbf{k}}^\mu \partial_\lambda G^{RA}(\mathbf{k}, \omega) v_{\mathbf{k}}^\nu \right]. \end{aligned} \quad (5)$$

Here, we use $\partial_\lambda = \partial / \partial k_\lambda$. We note the identity $\partial_\lambda G^{R/A} = G^{R/A} v_{\mathbf{k}}^\lambda$, which is useful for numerical calculations. Finally, we obtain the optical activity $\sigma_{\mu\nu\lambda}(\Omega) = \Phi_{\mu\nu\lambda}(\Omega) / i(\Omega + i\delta)$, where $\delta = +0$ is an adiabatic factor. This tensor $\sigma_{\mu\nu\lambda}$ describes all optical activity phenomena induced by the orbital moment, including the NOA and the OMEE. This formulation has been useful for analyses in periodic crystals as it avoids difficulties such as origin dependence and gauge invariance. Some works have derived this tensor with the band representation and proved explicitly that this formalism avoids these difficulties, providing a physical interpretation of the obtained gauge-invariant equations [21, 23, 27, 41, 42].

B. No-go theorem

The optical activity has a singularity at $\Omega = 0$ because of the factor $1/(\Omega + i\delta) = 1/\Omega - i\pi\delta(\Omega)$. This δ -function and the accompanying anomalous divergence scaling Ω^{-1} are known as the false divergences problem when using the velocity gauge from the minimal-coupling Hamiltonian [34]. This divergence is supposed to vanish in the normal state, which has been shown using the Bloch band representation [27]. We here clarify whether it also vanishes using the Green's function formula. The coefficient in front of the δ function in the optical activity reads

$$\Phi_{\mu\nu\lambda}(0) = i\varepsilon_{\mu\nu\lambda}\alpha. \quad (6)$$

Here, $\varepsilon_{\mu\nu\lambda}$ is the totally antisymmetric tensor. Almost all components of $\Phi_{\mu\nu\lambda}(0)$ are zero. Only totally antisymmetric terms appear due to α , which is real (see Appendix A for a detailed derivation). This term corresponds to the chiral magnetic effect, where a current density is induced by a magnetic field as $\mathbf{J} = \alpha\mathbf{B}$. However, this phenomenon usually does not occur unless, for example, the chiral chemical potential μ_5 is finite in the non-equilibrium case [43]. Using the Bloch band representation, this α is shown to be zero, resulting from

its topological nature [23, 27]. However, the formula using Green's function can not immediately prove that this term vanishes. Therefore, in the following discussion, we only consider cases where the chiral magnetic effect vanishes due to crystal point group symmetry.

III. ORBITAL OPTICAL ACTIVITY IN A SUPERCONDUCTOR

A. Green's function formula for a superconductor

In this paper, we treat the superconducting state using the mean-field approximation represented by the Bogoliubov-de Gennes (BdG) Hamiltonian as

$$H_{\text{BdG}} = \frac{1}{2} \sum_{\mathbf{k}nm} \psi_{n\mathbf{k}}^\dagger H_{\mathbf{k}nm}^{\text{BdG}} \psi_{m\mathbf{k}}, \quad (7a)$$

$$H_{\mathbf{k}nm}^{\text{BdG}} = \begin{pmatrix} H_{\mathbf{k}} - \mu & -\Delta_{\mathbf{k}} \\ -\Delta_{\mathbf{k}}^\dagger & -H_{-\mathbf{k}}^T + \mu \end{pmatrix}. \quad (7b)$$

Here, $\psi_{\mathbf{k}}^\dagger = (c_{1\mathbf{k}}^\dagger, \dots, c_{N\mathbf{k}}^\dagger, c_{1-\mathbf{k}}, \dots, c_{N-\mathbf{k}})$ is the Nambu spinor and $\Delta_{\mathbf{k}}$ is the pair potential, which is the order parameter of the superconducting state. We define M^T and M^\dagger as the transpose and the Hermitian conjugate of a matrix M . The current-current correlation function in the superconducting state is given by

$$\begin{aligned} \Phi_{\mu\nu}(\mathbf{q}, \Omega) &= \frac{e^2}{2} \int [d^4k] f(\omega) \text{Tr} \left[G_{\text{BdG}}^{RA}(\mathbf{k}-, \omega) \tilde{v}_{\mathbf{k}}^\mu G_{\text{BdG}}^R(\mathbf{k}+, \omega + \Omega) \tilde{v}_{\mathbf{k}}^\nu \right. \\ &\quad \left. + G_{\text{BdG}}^A(\mathbf{k}-, \omega - \Omega) \tilde{v}_{\mathbf{k}}^\mu G_{\text{BdG}}^{RA}(\mathbf{k}+, \omega) \tilde{v}_{\mathbf{k}}^\nu \right]. \quad (8) \end{aligned}$$

Here, $G_{\text{BdG}}^{R/A}(\mathbf{k}, \omega) = 1/(\omega - H_{\mathbf{k}}^{\text{BdG}} + \Sigma^{R/A}(\mathbf{k}, \omega))$ is the retarded/advanced Green's function for the BdG Hamiltonian, including the self-energy describing the dissipation effect. A specific equation of this self-energy will be given in a model calculation below. The velocity operator is different from the normal state. It is given by

$$\tilde{v}_{\mathbf{k}}^\mu = \begin{pmatrix} v_{\mathbf{k}}^\mu & 0 \\ 0 & -(v_{-\mathbf{k}}^\mu)^T \end{pmatrix}. \quad (9)$$

We note that this velocity operator is not the usual derivative of the BdG Hamiltonian $H_{\mathbf{k}}^{\text{BdG}}$ by the wavenumber \mathbf{k} . Expanding the correlation function by \mathbf{q} , the first-order term is

$$\begin{aligned} \Phi_{\mu\nu\lambda}(\Omega) &= \frac{e^2}{4} \int [d^4k] f(\omega) \\ &\quad \times \text{Tr} \left[-\partial_\lambda G_{\text{BdG}}^{RA}(\mathbf{k}, \omega) \tilde{v}_{\mathbf{k}}^\mu G_{\text{BdG}}^R(\mathbf{k}, \omega + \Omega) \tilde{v}_{\mathbf{k}}^\nu \right. \\ &\quad + G_{\text{BdG}}^{RA}(\mathbf{k}, \omega) \tilde{v}_{\mathbf{k}}^\mu \partial_\lambda G_{\text{BdG}}^R(\mathbf{k}, \omega + \Omega) \tilde{v}_{\mathbf{k}}^\nu \\ &\quad - \partial_\lambda G_{\text{BdG}}^A(\mathbf{k}, \omega - \Omega) \tilde{v}_{\mathbf{k}}^\mu G_{\text{BdG}}^{RA}(\mathbf{k}, \omega) \tilde{v}_{\mathbf{k}}^\nu \\ &\quad \left. + G_{\text{BdG}}^A(\mathbf{k}, \omega - \Omega) \tilde{v}_{\mathbf{k}}^\mu \partial_\lambda G_{\text{BdG}}^{RA}(\mathbf{k}, \omega) \tilde{v}_{\mathbf{k}}^\nu \right]. \quad (10) \end{aligned}$$

The derivative of the Green's function by the wavenumber can be transformed into the useful form for numerical calculations as $\partial_\lambda G_{\text{BdG}}^{R/A} = G_{\text{BdG}}^{R/A} \hat{v}_{\mathbf{k}}^\lambda G_{\text{BdG}}^{R/A}$, where

$$\hat{v}_{\mathbf{k}}^\lambda = \frac{\partial H_{\mathbf{k}}^{\text{BdG}}}{\partial k_\lambda} = \begin{pmatrix} v_{\mathbf{k}}^\lambda & -\partial_\lambda \Delta_{\mathbf{k}} \\ -\partial_\lambda \Delta_{\mathbf{k}}^\dagger & (v_{-\mathbf{k}}^\lambda)^T \end{pmatrix}. \quad (11)$$

This velocity operator \hat{v} is different from \tilde{v} even if the pair potential is independent of the wavenumber. Finally, we obtain the optical activity for the superconducting state by $\sigma_{\mu\nu\lambda}(\Omega) = \Phi_{\mu\nu\lambda}(\Omega)/i(\Omega + i\delta)$.

B. Singularity and relation to the superconducting Edelstein effect

In the previous section, we have shown that the optical activity appears to have a δ -function singularity at $\Omega = 0$, which, however, vanishes in the normal state. In the superconducting case, the singularity generally is finite. The absence of cancellation is attributed to the difference in the velocity operator from the normal state. The coefficient of the δ function satisfies (see Appendix A for a detailed derivation)

$$\Phi_{\mu\nu\lambda}(0) = \tilde{\Phi}_{\mu\nu\lambda} - (\mu \leftrightarrow \nu). \quad (12)$$

$\tilde{\Phi}_{\mu\nu\lambda}$ is purely imaginary, and its detailed form is discussed in Appendix A. $\Phi_{\mu\nu\lambda}(0)$ is antisymmetric for the interchange between μ and ν . Being purely imaginary is consistent with the general symmetry argument for a current-current correlation function [40]. Therefore, the δ -function singularity appears in the imaginary part of the optical activity $\text{Im}\sigma_{\mu\nu\lambda}(\Omega)$, and the anomalous $1/\Omega$ divergence with the same coefficient $\Phi_{\mu\nu\lambda}(0)$ as the δ -function singularity appears in the real part $\text{Re}\sigma_{\mu\nu\lambda}(\Omega)$ to satisfy the Kramers-Kronig relation. Due to the antisymmetry in the indices μ and ν , the anomalous term only appears in the NOA. The OMEE does not exhibit this singularity because the OMEE originates from the symmetric part of the interchange between μ and ν due to the necessity of the time-reversal symmetry breaking. Such anomalous frequency dependence is common in superconductors. The optical conductivity has the same anomaly, and the coefficient corresponds to the superfluid density [44]. Furthermore, it has recently been shown that also the nonlinear conductivity has a similar anomaly, and the coefficient has the meaning of the nonreciprocal superfluid density [45, 46]. The physical meaning of the coefficient in the case of the optical activity is also known. It has been studied for the spin contribution, and the coefficient corresponds to the superconducting Edelstein effect [20, 22, 40]. In this paper, we consider the orbital contribution, and we will reveal the physical meaning of $\Phi_{\mu\nu\lambda}(0)$ in the following discussion.

$\Phi_{\mu\nu\lambda}(0)$ has nine components due to its antisymmetric property. Therefore, it can be rewritten by a rank-2

tensor $\mathcal{K}_{\mu\nu}$ with a one-to-one correspondence [21, 47] as

$$\Phi_{\mu\nu\lambda}(0) = i\varepsilon_{\mu\lambda\theta}\mathcal{K}_{\nu\theta} - i\varepsilon_{\nu\lambda\theta}\mathcal{K}_{\mu\theta}, \quad (13a)$$

$$\mathcal{K}_{\mu\nu} = -\frac{1}{4i}\varepsilon_{\nu\theta\lambda}\left(2\Phi_{\mu\theta\lambda}(0) - \Phi_{\theta\lambda\mu}(0)\right). \quad (13b)$$

Here, $\mathcal{K}_{\mu\nu}$ is real because $\Phi_{\mu\nu\lambda}(0)$ is purely imaginary. Substituting Eq. (13a) into the original linear response relation, we obtain

$$J_\mu = \mathcal{K}_{\mu\theta}B_\theta + (i\mathbf{q} \times \mathbf{M})_\mu, \quad M_\theta = \mathcal{K}_{\mu\theta}A_\mu. \quad (14)$$

\mathcal{K} represents the superconducting Edelstein effect (SEE), where a supercurrent induces a magnetization \mathbf{M} or the magnetic field \mathbf{B} induces the supercurrent. Thus, $\Phi_{\mu\nu\lambda}(0)$ also has the physical meaning of the SEE for the orbital contribution, in analogy to the case of the spin contribution.

Previous works about the SEE [48–53] have mainly focused on the induced spin moment in systems with spin-orbit coupling (SOC). Recently, supercurrent-induced orbital magnetization has been proposed [54] and is expected to appear in systems where the valley degrees of freedom are of key importance, such as the transition metal dichalcogenides (TMDs) and twisted bilayer graphene (TBG), even without SOC. The SEE is a unique response for noncentrosymmetric superconductors and is expected to provide essential information about them; however, it has not been observed in experiments for both spin and orbital parts.

Here, we propose another means of observing this SEE. By measuring the spectrum of the optical activity, we can obtain $\Phi_{\mu\nu\lambda}(0)$, which is equivalent to the SEE. $\Phi_{\mu\nu\lambda}(0)$ can be obtained by measuring the coefficient of the anomalous divergence of $\text{Re}\sigma_{\mu\nu\lambda}(\Omega)$ scaling as Ω^{-1} . Furthermore, the spectrum of $\text{Im}\sigma_{\mu\nu\lambda}(\Omega)$ can also determine the value of $\Phi_{\mu\nu\lambda}(0)$. Reference [40] has shown that the missing area, the area reduced from the spectrum of the normal phase created by the superconducting gap, is identical to $\Phi_{\mu\nu\lambda}(0)$ because of a universal sum rule and the no-go theorem in the case of the spin contribution. This method is useful for dirty superconductors, which is a common situation. As discussed in Sec. II B, the no-go theorem is also established for the orbital contribution. Thus, the missing area measurement is also valid for the orbital contribution.

IV. MODEL CALCULATION IN THE NORMAL STATE

In this section, we discuss the orbital optical activity using a model Hamiltonian to investigate the characteristics of the spectrum.

A. Optical activity in the normal state

We discuss the orbital optical activity in the normal state. We use a model Hamiltonian imitating strained

MoS₂. For simplicity, we ignore the SOC, which is realized in the conduction band of MoS₂ [55, 56]. In this case, the spin part of the optical activity vanishes, and the orbital part plays the central role.

The Hamiltonian is written as

$$H_{\mathbf{k}} = \begin{pmatrix} G & \epsilon_{\mathbf{k}} \\ \epsilon_{\mathbf{k}}^* & -G \end{pmatrix} \otimes \sigma_0, \quad (15a)$$

$$\epsilon_{\mathbf{k}} = te^{i\mathbf{k}\cdot\mathbf{a}_1} + t'(e^{i\mathbf{k}\cdot\mathbf{a}_2} + e^{i\mathbf{k}\cdot\mathbf{a}_3}). \quad (15b)$$

Here, t and t' are hopping parameters, and G is the gap parameter that opens a gap at the K and K' points due to spatial inversion symmetry breaking. We use $\mathbf{a}_1 = (0, 1/\sqrt{3})$, $\mathbf{a}_2 = (-1/2, -1/2\sqrt{3})$ and $\mathbf{a}_3 = (1/2, -1/2\sqrt{3})$, and we set the lattice constant $a = 1$ ($a = 2.4$ Å for MoS₂). σ_0 is the identity matrix for the spin degrees of freedom. In the following, we set $t > t'$ to incorporate the effect of stretching in the x direction. We plot the band structure in the left panel of Fig. 1. The Hamiltonian belongs to the point group C_{2v} . Therefore, the Edelstein effect and the orbital optical activity are restricted to the one component χ_{xz} , where $J_\mu = -\chi_{\mu\nu}\dot{B}_\nu$ and $M_\nu = \chi_{\mu\nu}E_\mu$. Then, the nonzero component of the optical activity tensor is only $\sigma_{xyx} = -\sigma_{yxx}$ and is related to $\chi_{xz} = -i\sigma_{xyx}$ [57]. The stretching generates the in-plane polarization and the induced out-of-plane magnetization. This type of optical activity is different from the case of the chiral-structured materials, where the induced magnetization is parallel to the electric field [34, 58].

We show the numerical results of the optical activity σ_{xyx} in the middle and right panels of Fig. 1 (blue lines). We use $t = 1$ eV, $t' = 0.9t$, $G = 0.2t$, $\mu = 0.5t$, and $\Gamma = 0.1t$. At frequencies smaller than the dissipation, $\Omega < \Gamma$, intraband transitions are dominant and show a Drude model-like behavior. In this region, the imaginary part of the optical activity is larger than the real part, and the real part is linear in the frequency and becomes comparable with the imaginary part when the frequency reaches the scale of the dissipation. This behavior is identical to that of the uniform optical conductivity described by the Drude model. It is consistent with the equation of the gyrotropic magnetic effect (GME) in a nonabsorbing regime [23]. This effect originates from the orbital magnetic moment dipole (OMMD)

$$\int_{\text{BZ}} \frac{d^d k}{(2\pi)^d} \sum_n f(\epsilon_{n\mathbf{k}} - \mu) \partial_{k_i} m_{n\mathbf{k}}^{\text{orb}}, \quad (16)$$

where $m_{n\mathbf{k}}^{\text{orb}}$ is the orbital magnetic moment oriented in the direction perpendicular to the surface. Without stretching MoS₂, orbital magnetic moments (OMMs) with opposite signs exist around the K and K' points [59]; however, the OMMD vanishes due to C_{3v} symmetry. When stretching MoS₂, the OMMD in the same direction as the stretching direction becomes finite and generates the GME. This discussion is similar to the Berry curvature dipole in the nonlinear Hall effect [60]. The GME

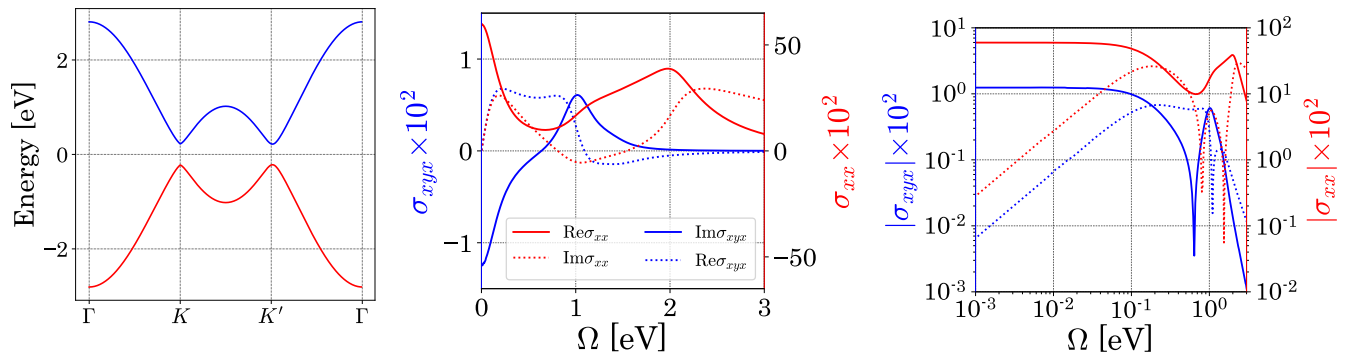


FIG. 1. (Left) Band structure of the used model: We set $t = 1\text{eV}$, $t' = 0.9t$, and $G = 0.2t$. (Middle) Numerical results of the orbital optical activity σ_{xyx} (blue lines and left axis) and the optical conductivity σ_{xx} (red lines and right axis): We set $t = 1\text{eV}$, $t' = 0.9t$, $G = 0.2t$, $\mu = 0.5t$, and $\Gamma = 0.1t$. (Right) The magnitude of σ_{xyx} and σ_{xx} is plotted on a logarithmic scale. The lines are the same as in the middle panel. We set σ_{xyx} and σ_{xx} in units of $e^2 a/\hbar$ and e^2/\hbar .

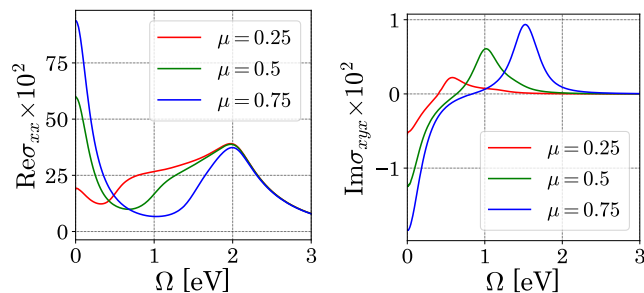


FIG. 2. Chemical potential dependence of the optical conductivity (Left) and the optical activity (Right). We use the same parameters and units as in Fig. 1.

in the DC limit has been experimentally observed as the orbital Edelstein effect in stretched MoS_2 [61, 62]. Above the frequency corresponding to the optical gap $\sim 2\mu$, interband effects become finite around K and K' points.

For the following discussion, we also calculate the optical conductivity. In Fig. 1 (red lines), we plot the numerical results of the longitudinal optical conductivity σ_{xx} . The character of this spectrum is similar to the optical activity. In the low-frequency regime, $\Omega < \Gamma$, the optical conductivity follows the Drude theory. The magnitude of the conductivity in the DC limit is $0.6e^2/\hbar$, which is comparable to a dual-gated monolayer MoS_2 [63]. Above the frequency corresponding to the optical gap ($\sim 2\mu$), interband transitions appear, and the spectrum forms a Lorentz-peak structure.

However, a clear difference from the optical activity can be identified. We can see that the interband peak position differs between $\text{Im}\sigma_{xyx}$ and $\text{Re}\sigma_{xx}$. The peaks are located at $\Omega = 1\text{ eV}$ and $\Omega = 2\text{ eV}$, respectively. This distinction becomes clearer when looking at the chemical potential dependence in Fig. 2. While the interband peak of the optical conductivity $\text{Re}\sigma_{xx}$ does not depend on the chemical potential and is located at $\Omega = 2\text{ eV}$, the interband peak in the optical activity $\text{Im}\sigma_{xyx}$ shifts

as the chemical potential is increased. It is located at the optical gap 2μ . The typical optical transition occurs as a transition from an occupied state to an unoccupied state. Thus, the spectra should match once the optical gap is exceeded. The spectra of $\text{Re}\sigma_{xx}$ are indeed identical among different chemical potentials above the optical gap 2μ ; however, the spectra of $\text{Im}\sigma_{xyx}$ behave differently. In the following, we explain the reason for these distinctions.

The interband transition peak is often explained by the joint density of states (JDOS). The JDOS is defined by

$$J(\Omega) = \int_{\text{BZ}} \frac{d^d k}{(2\pi)^d} \delta(\Omega - \Delta\epsilon_{\mathbf{k}}). \quad (17)$$

Here, $\Delta\epsilon_{\mathbf{k}} = \epsilon_{\mathbf{k}}^c - \epsilon_{\mathbf{k}}^v$ is the energy difference between the conduction band and the valence band. Thus, the JDOS has a maximum at the frequency where the largest number of states can be excited. In this paper, to account for the broadening of the DOS due to dissipation, we substitute the δ function by the Lorentz function as $\delta(x) \sim \Gamma/(\pi^2 x^2 + \Gamma^2)$, where Γ is the dissipation used in the calculation of Fig. 1. We show the numerical results of the JDOS in the left panel of Fig. 3. The JDOS has a maximum around $\Omega = 2\text{ eV}$, explaining the optical conductivity's peak. However, the JDOS cannot explain the peak shift of the optical activity.

This peak shift is unique to the orbital optical activity in metals. It becomes clearer when the optical activity is represented by the Bloch band basis. The full representation is derived in a recent work [27] (see Eq. (26) in the paper). It shows that there is a Fermi surface effect affecting the interband transition besides the Fermi sea effect. This is unique to the orbital contribution. It demonstrates that the effect of optical transitions in the optical activity cannot be simply described by transitions from occupied to unoccupied states, which is described by the Fermi sea term. We note that in this two-band model with particle-hole symmetry, the Fermi sea term is suppressed. The Fermi surface term is locally enhanced

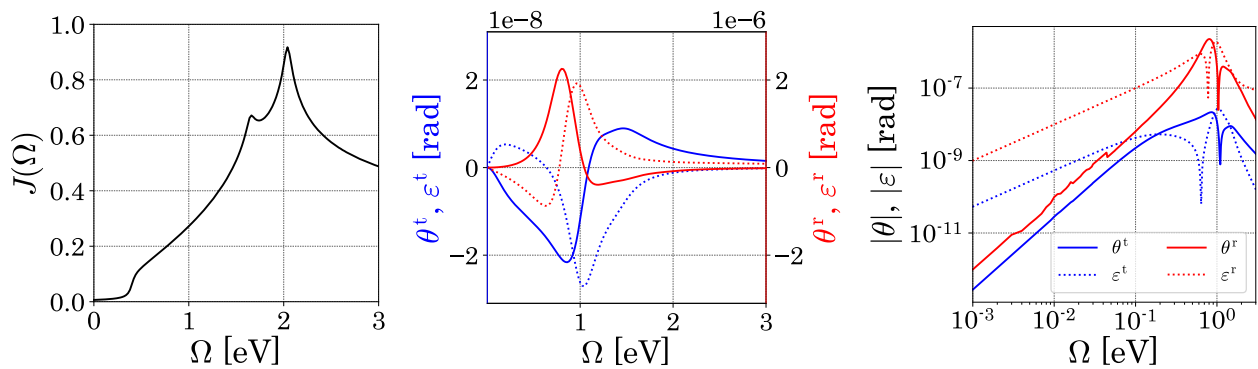


FIG. 3. (Left) Numerical results of the JDOS, $J(\Omega)$. We use the same parameters as in Fig. 1. (Middle) Numerical results of the optical rotational angle θ and the ellipticity ε . The red and blue lines correspond to the reflected light (right axis) and the transmitted light (left axis). The legend is identical to the right panel. We use the same parameters as in Fig. 1. (Right) The magnitude of θ and ε is plotted on a logarithmic scale.

at the optical gap 2μ , which is consistent with the result in Fig. 2.

B. Optical Kerr effect

The optical activity σ_{xyx} in our model can be observed using the optical Kerr effect. The Kerr effect is usually caused by the optical Hall effect in magnets without time-reversal symmetry. Because the present model obeys time-reversal symmetry, the Kerr effect originating from the optical Hall effect does not occur. However, the optical activity also generates an optical Kerr effect by a different mechanism, as described in the following discussion.

The spectrum of the longitudinal optical conductivity $\sigma_{ii}(\omega)$ can be extracted from the experimentally observed complex reflectance. Similarly, the spectrum of the optical activity can be extracted from the experimentally observed rotational angle and the ellipticity caused by the Kerr effect or the Faraday effect. In two-dimensional materials, transmission through the material does not exist, and thus, only the Kerr effect is allowed. In this subsection, we discuss the Kerr effect as a possibility of observing the optical activity experimentally.

We consider an electromagnetic wave incident in the xz plane at an angle of incidence of 45° (see Appendix B for a detailed discussion and calculation). The two-dimensional material is put on the $z = 0$ plane, and the incident electric field is assumed to be s -polarized, i.e., pointing in the y -axis direction. Then, the reflected electric field, (E_y^r, E_{xz}^r) , and the transmitted electric field, (E_y^t, E_{xz}^t) , satisfy the following ratio

$$\frac{E_{xz}^r}{E_y^r} \sim \frac{\Omega \sigma_{xyx}}{c(\mu_0 c \sigma_{yy})} \left(\frac{2\sqrt{2}}{\mu_0 c} + \sigma_{xx} \right)^{-1}, \quad (18)$$

$$\frac{E_{xz}^t}{E_y^t} = -\frac{\Omega \sigma_{xyx}}{\sqrt{2}c} \left(\frac{2\sqrt{2}}{\mu_0 c} + \sigma_{xx} \right)^{-1}. \quad (19)$$

Here, we ignore the squared term of σ_{xyx} in Eq. (18) because it is very small. μ_0 and c are the permeability of the vacuum and the light velocity, and the product of them $(\mu_0 c)^{-1} \sim 10.90e^2/\hbar$ is the inverse of the vacuum impedance. Usually, a two-dimensional material is attached to a substrate. We assume that the refractive index of the substrate at the frequency of interest is 1 in this paper. The component $E_{xz}^{r,t}$ is the transverse response induced by the magnetoelectric effect $\chi_{xz} = -i\sigma_{xyx}$, and it is perpendicular to the usual response $E_y^{r,t}$. Thus, the output electric field is no longer linearly polarized, but, in general, it becomes an ellipse whose deflection direction is tilted from the y axis. The ratio relations in Eqs. (18) and (19) give the ratio of the magnitude and the phase difference between electric fields perpendicular to each other. They determine the rotational angle θ and the ellipticity ε of the output electric fields (see Appendix B for the equation of θ and ε). We show the rotational angle and the ellipticity in the middle and right panels in Fig. 3 using the data of Fig. 1. The Kerr effect is enhanced at $\Omega = 1$ eV corresponding to the peak of the optical activity. Its magnitude reaches about 2 μ rad for the reflected light and 20 nrad for the transmitted one. We see that in the low-frequency regime, the ellipticity predominates because the optical conductivity is dominated by the real part, and the optical activity is dominated by the imaginary part. In other words, the phases of these two electric fields exhibit a deviation of nearly $\pi/2$ from each other. Its magnitude decreases, reaching about $\varepsilon^r \sim 1$ nrad and $\varepsilon^t \sim 0.05$ nrad at $\Omega = 1$ meV.

Next, we comment on the order of the ellipticity for real two-dimensional materials such as doped monolayer TMDs and TBG in the low-frequency regime. The conductivity of TMDs and TBG is $10e^2/\hbar$ at the maximum [63–66]. Thus, it is smaller or comparable to $(\mu_0 c)^{-1}$. Therefore, the ellipticity of the reflection light in this regime is approximately written as $k\chi'/\sigma'$, where k is the wavenumber of the light, χ' is the real part of $\chi_{\mu\nu}$, and σ' is the real part of the conductivity. This equa-

tion is the Edelstein coefficient $\alpha = \chi'/\sigma'$ multiplied by the wavenumber. For strained MoS₂ with 1% strain, the Edelstein coefficient is observed to be $\alpha = 0.1 \text{ \AA}$ [61]. Thus, the ellipticity is converted to $\varepsilon^r = 8 \text{ mrad}$ for the frequency $\Omega = 1 \text{ meV}$ (i.e. $k = 8 \text{ cm}^{-1}$), which is comparable to our calculation. For TBG [54], the Edelstein coefficient is expected to be larger, reaching 10 \AA . Thus, the ellipticity will be 0.8 \mu rad at $\Omega = 1 \text{ meV}$.

V. MODEL CALCULATION IN THE SUPERCONDUCTING STATE

In this section, we discuss the optical activity in the superconducting state. We use the same Hamiltonian $H_{\mathbf{k}}$ mimicking strained MoS₂ as in Sec. IV. We assume that the superconducting state is a uniform singlet. Thus, we introduce the pair potential as $\Delta_{\mathbf{k}} = \Delta\tau_0 \otimes i\sigma_y$, where Δ is real and τ_0 is the identity matrix for the sublattice degrees of freedom. When calculating the optical conductivity and the optical activity using Green's functions (Eq. 10), we introduce the dissipation effect phenomenologically. For this purpose, we introduce the renormalization factor

$$\eta_\omega = 1 + \Gamma \left(\frac{\theta(|\Delta| - |\omega|)}{\sqrt{\Delta^2 - \omega^2}} + \frac{i \text{sign}(\omega)\theta(|\omega| - |\Delta|)}{\sqrt{\omega^2 - \Delta^2}} \right), \quad (20)$$

where $\theta(x)$ is the step function and $\text{sign}(x)$ is the sign function returning $+1$ if $x > 0$ and -1 if $x < 0$. Then, we treat the dissipation effect by impurities as replacing ω and Δ in the Green's function $G_{\text{BdG}}^{R/A}(\mathbf{k}, \omega)$ by $\eta_\omega\omega$ and $\eta_\omega\Delta$. This renormalization is derived from the Born approximation [67]. In the limit $\Delta \rightarrow 0$, it is consistent with a constant dissipation $i\Gamma$ used in the calculations in the normal state.

We show the numerical results of the optical activity σ_{xyx} and the optical conductivity σ_{xx} of the superconducting state in Fig. 4 (solid lines). We also include the results of the normal state for comparison (dashed lines). The spectra differ from the normal state below $\Omega = 2\Delta = 0.01$. $\text{Im}\sigma_{xyx}$ and $\text{Re}\sigma_{xx}$ decay rapidly with decreasing frequency around 2Δ , and the weights become zero in the gap. This difference in the spectra from the normal state is called the missing area. $\text{Re}\sigma_{xyx}$ and $\text{Im}\sigma_{xx}$ are enhanced in the gap and follow a Ω^{-1} dependence. The missing area and the anomalous divergence indicate the existence of a condensation. In particular, the missing area of the optical conductivity is known as the Ferrell-Glover-Tinkham sum rule for measuring the superfluid density [68, 69]. Similarly, they can be used to measure the SEE by the optical activity as discussed in Sec. III B.

The Kerr rotation and ellipticity are also changed because of the spectral modification by the superconducting state. We show the Kerr rotation θ and ellipticity ε in Fig. 5 (blue lines). We also show the results of the normal state for comparison (black lines). As discussed in Sec. IV B, in the normal state, Eqs. (18) and (19) are

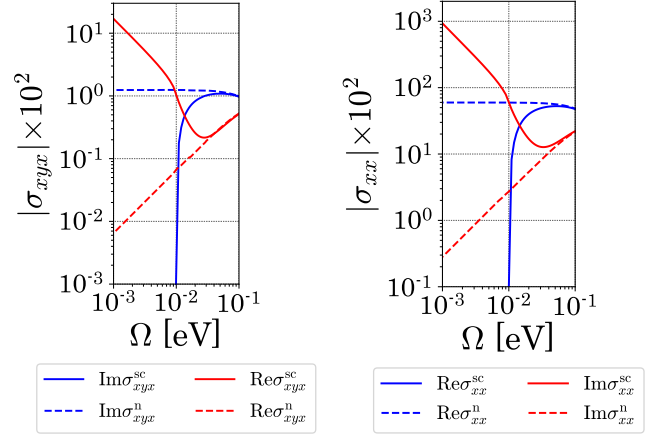


FIG. 4. Numerical results of the optical activity σ_{xyx} (Left) and the optical conductivity σ_{xx} (Right) in the superconducting state on a logarithmic scale. We denote the superconducting state and the normal state as sc and n, respectively. We use the same parameters and units as in Fig. 1. We set $\Delta = 0.005$.

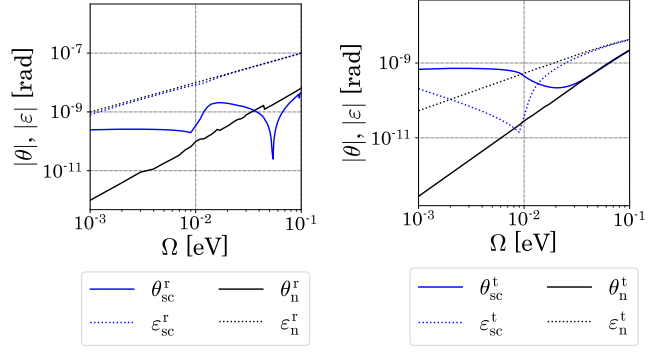


FIG. 5. Numerical results of the Kerr rotation θ and ellipticity ε for the reflected light (Left) and the transmitted light (Right) on a logarithmic scale. We denote the superconducting state and the normal state as sc and n, respectively. We use the same parameters and units as in Fig. 1. We set $\Delta = 0.005$.

almost purely imaginary in the Drude regime. Thus, the phase difference of the electric fields is almost $\pi/2$, and the ellipticity is dominant. In the superconducting state, for frequencies inside the superconducting gap, the dominant components of $\sigma_{xx/yy}$ and σ_{xyx} are changed to the imaginary part and the real part, respectively. Therefore, Eq. (18) is no longer purely imaginary, and the Kerr rotation is enhanced. At low frequencies, $\text{Im}\sigma_{xx}$ increases by Ω^{-1} and becomes comparable to the inverse vacuum impedance $(\mu_0 c)^{-1}$. Then, the real part and imaginary part of Eq. (18) are comparable, and the rotational angle and ellipticity are in the same order of magnitude for the reflected light. For transmitted light, Eq. (19) is also no longer purely imaginary and becomes rather real when $(\mu_0 c)^{-1} > \text{Im}\sigma_{xx}$, thus the rotational angle is dominant. As the frequency decreases further, $\text{Im}\sigma_{xx}$ increases by

Ω^{-1} and becomes comparable to $(\mu_0 c)^{-1}$. Then, the rotational angle and the ellipticity also become comparable in magnitude.

VI. CONCLUSION AND DISCUSSION

In this paper, we have discussed the optical activity originating from the orbital magnetic moment in metals and superconductors using a Green's function formalism. We have shown that the no-go theorem in the normal state, stating that a singular contribution to the optical activity is absent, is valid except for the chiral magnetic effect and that this theorem is broken for the superconducting state in Secs. II and III. Then, this singularity contributes to the δ function in $\text{Im}\sigma_{\mu\nu\lambda}$ in the DC-limit and the anomalous Ω^{-1} -divergence in $\text{Re}\sigma_{\mu\nu\lambda}$ for superconductors. In the superconducting state, the coefficient of the singular part is confirmed to be exactly the superconducting Edelstein effect (SEE), which implies the validity of the missing area measurement for the SEE. An identical discussion was recently presented for the spin-induced optical activity. In this paper, it has been shown that the same discussion holds for the orbital-induced optical activity. In Sec. IV, we have shown calculations using a model for monolayer TMDs. We have used an effective two-band model to elucidate the typical behavior of the optical activity. We have revealed that the low-frequency spectrum is described by a Drude-like model and that the interband transition shows an atypical chemical potential dependence originating from the interband Fermi surface term, unique to the orbital part in metals. In addition, we have evaluated the Kerr spectrum. In Sec. V, we have calculated the spectrum of the optical activity in the superconducting state, and we have demonstrated the existence of the missing area and the anomalous divergence of the optical activity at low frequencies. In addition, we have discussed the modification of the Kerr effect by the superconducting state.

Finally, we discuss the possibility of an experimental realization separated into the interband regime and the intraband regime. As discussed in Sec. IV, the interband peak is located at about a few eV. The Kerr rotation and ellipticity for the reflected light reach a few μrad , which makes them detectable with the state-of-the-art instru-

ments, having a resolution of 10 nrad [70, 71]. On the other hand, the resolution in the terahertz regime, corresponding to the gap scale of most noncentrosymmetric superconductors, has recently been reported to reach 20 μrad and is expected to go down to 2 μrad [72]. The Kerr effect of TBG is close to this technical observable limit. Thus, unless we can find other two-dimensional materials with a larger Edelstein coefficient α , the experimental observation is currently challenging in this regime.

Finally, we shortly discuss the three-dimensional materials. In three-dimensional systems, the Faraday effect is expected. As light cannot easily penetrate superconductors, transmission can only occur in thin films [73]. The Faraday effect originates from the difference of the refractive index for left and right circular polarized lights Δn . It is given by $\Phi_F (= \theta_F + i\varepsilon_F) = -\Delta n k \zeta / 2$, where θ_F and ε_F are the rotational angle and the ellipticity for the Faraday effect, k is the wavenumber of the light, and ζ is the thickness of materials. For the natural optical activity, the refractive index difference is given by $\Delta n = \mu_0 c \chi$ [74]; thus, we can directly obtain the spectrum of the optical activity χ from the Faraday spectrum. In the case of noncentrosymmetric cubics (point group: O and T), the optical activity in the THz regime is $\chi \sim (e\mu_B \tau k_F^2 / \hbar)(\gamma k_F / E_F)$ with an antisymmetric SOC term $\gamma \mathbf{k} \cdot \boldsymbol{\sigma}$. Here, μ_B is the Bohr magneton, τ is the relaxation time, and k_F and E_F are the Fermi wavenumber and the Fermi energy. Candidates for superconductors with this SOC include $\text{Li}_2\text{Pd}_3\text{B}$, $\text{Li}_2\text{Pt}_3\text{B}$, and $\text{Mo}_2\text{Al}_3\text{C}$ [75]. Then, the Faraday effect reads

$$\Phi_F \sim -\frac{1}{2} \frac{e\mu_B \mu_0 k_F}{\hbar} (\Omega \tau) (k_F \zeta) \frac{\gamma k_F}{E_F}, \quad (21)$$

and the typical order of magnitude is estimated to be 4.8 μrad for $k_F = 1 \text{ \AA}^{-1}$, $\tau = 10 \text{ fs}$, and $\gamma k_F / E_F = 10^{-2}$ at $\Omega = 1 \text{ THz}$ using the thickness $\zeta = 500 \text{ \AA}$.

ACKNOWLEDGEMENTS

K.S. acknowledges support as a JSPS research fellow and is supported by JSPS KAKENHI, Grant No.22J23393 and No.22KJ2008. R.P. is supported by JSPS KAKENHI No.23K03300.

Appendix A: No-go theorem

The singular part of the optical activity is restricted in the normal state. This part was shown to be forbidden for the spin contribution [40]. In this appendix, we will show that the part for the orbital part is also restricted. The

coefficient of the singular part is

$$\begin{aligned}
\Phi_{\mu\nu\lambda}(0) &= \frac{e^2}{2} \int [d^4k] f(\omega) \text{Tr} \left[-\partial_\lambda G^{RA}(\mathbf{k}, \omega) v_{\mathbf{k}}^\mu G^R(\mathbf{k}, \omega) v_{\mathbf{k}}^\nu + G^{RA}(\mathbf{k}, \omega) v_{\mathbf{k}}^\mu \partial_\lambda G^R(\mathbf{k}, \omega) v_{\mathbf{k}}^\nu \right. \\
&\quad \left. - \partial_\lambda G^A(\mathbf{k}, \omega) v_{\mathbf{k}}^\mu G^{RA}(\mathbf{k}, \omega) v_{\mathbf{k}}^\nu + G^A(\mathbf{k}, \omega) v_{\mathbf{k}}^\mu \partial_\lambda G^{RA}(\mathbf{k}, \omega) v_{\mathbf{k}}^\nu \right] \\
&= \frac{e^2}{2} \int [d^4k] f(\omega) \text{Tr} \left[-\partial_\lambda G^R(\mathbf{k}, \omega) v_{\mathbf{k}}^\mu G^R(\mathbf{k}, \omega) v_{\mathbf{k}}^\nu + G^R(\mathbf{k}, \omega) v_{\mathbf{k}}^\mu \partial_\lambda G^R(\mathbf{k}, \omega) v_{\mathbf{k}}^\nu \right. \\
&\quad \left. + \partial_\lambda G^A(\mathbf{k}, \omega) v_{\mathbf{k}}^\mu G^A(\mathbf{k}, \omega) v_{\mathbf{k}}^\nu - G^A(\mathbf{k}, \omega) v_{\mathbf{k}}^\mu \partial_\lambda G^A(\mathbf{k}, \omega) v_{\mathbf{k}}^\nu \right] \\
&= e^2 \int [d^4k] f(\omega) \text{ReTr} \left[-\partial_\lambda G^R(\mathbf{k}, \omega) v_{\mathbf{k}}^\mu G^R(\mathbf{k}, \omega) v_{\mathbf{k}}^\nu + G^R(\mathbf{k}, \omega) v_{\mathbf{k}}^\mu \partial_\lambda G^R(\mathbf{k}, \omega) v_{\mathbf{k}}^\nu \right]. \tag{A1}
\end{aligned}$$

Here, $\int [d^4k] = \int_{-\infty}^{\infty} d\omega / (2\pi i) \int_{\text{BZ}} d^3k / (2\pi)^3$. Thus, this equation is purely imaginary. Using the relation $\partial_\lambda G^R(\mathbf{k}, \omega) = G^R(\mathbf{k}, \omega) v_{\mathbf{k}}^\lambda G^R(\mathbf{k}, \omega)$, we obtain

$$\begin{aligned}
\Phi_{\mu\nu\lambda}(0) &= e^2 \int [d^4k] f(\omega) \text{ReTr} \left[-G^R(\mathbf{k}, \omega) v_{\mathbf{k}}^\lambda G^R(\mathbf{k}, \omega) v_{\mathbf{k}}^\mu G^R(\mathbf{k}, \omega) v_{\mathbf{k}}^\nu + G^R(\mathbf{k}, \omega) v_{\mathbf{k}}^\mu G^R(\mathbf{k}, \omega) v_{\mathbf{k}}^\lambda G^R(\mathbf{k}, \omega) v_{\mathbf{k}}^\nu \right] \\
&= e^2 \varepsilon_{\mu\nu\lambda} \int [d^4k] f(\omega) \text{ReTr} \left[-G^R(\mathbf{k}, \omega) v_{\mathbf{k}}^x G^R(\mathbf{k}, \omega) v_{\mathbf{k}}^y G^R(\mathbf{k}, \omega) v_{\mathbf{k}}^z + G^R(\mathbf{k}, \omega) v_{\mathbf{k}}^y G^R(\mathbf{k}, \omega) v_{\mathbf{k}}^x G^R(\mathbf{k}, \omega) v_{\mathbf{k}}^z \right]. \tag{A2}
\end{aligned}$$

This equation is totally antisymmetric. Then, we show that most components vanish. Only the totally antisymmetric part remains. This remaining part is known to be the chiral magnetic effect, as mentioned in the main text. It can be shown that this part is also zero by its topological nature using the band representation [23, 27].

In the superconducting case, this no-go theorem changes. Calculating the singular term in the same way, we obtain

$$\Phi_{\mu\nu\lambda}(0) = \frac{e^2}{2} \int [d^4k] f(\omega) \text{ReTr} \left[-\partial_\lambda G_{\text{BdG}}^R(\mathbf{k}, \omega) \tilde{v}_{\mathbf{k}}^\mu G_{\text{BdG}}^R(\mathbf{k}, \omega) \tilde{v}_{\mathbf{k}}^\nu + G_{\text{BdG}}^R(\mathbf{k}, \omega) \tilde{v}_{\mathbf{k}}^\mu \partial_\lambda G_{\text{BdG}}^R(\mathbf{k}, \omega) \tilde{v}_{\mathbf{k}}^\nu \right]. \tag{A3}$$

This equation is purely imaginary and antisymmetric under the interchange between μ and ν . However, there is one difference to the case of the normal state. The velocity operator appearing by differentiating the Green's function $\tilde{v}_{\mathbf{k}}^\mu$ is different from the velocity operator $v_{\mathbf{k}}^\mu$. Thus, many components of the singular part can be finite.

Appendix B: Optical Kerr effect

Here, we derive the rotational angle in two-dimensional metals with an in-plane polar axis pointing in the x direction. In this case, the in-plane current induces the out-of-plane magnetization, which is often discussed in strained TMDs and twisted bilayer graphene. In the following, we consider that the two-dimensional metal is put on an insulating substrate, which has a real-valued refractive index n_{sub} in the frequency regime of interest, and we assume $n_{\text{sub}} \sim 1$.

We will derive the rotational angle using Maxwell's electrodynamics. We consider that the incident light is in the xz plane and travels at an angle of incidence of 45° . Furthermore, the electric field of the incident light is the s -polarized and, thus, is oriented in the y direction. In this case, the electric field for the incident light \mathbf{E}^{in} , the reflected light \mathbf{E}^{r} , and the refracted light \mathbf{E}^{t} are given

by

$$\mathbf{E}^{\text{in}} = E^{\text{in}} \mathbf{e}_y e^{i\mathbf{k}\cdot\mathbf{r} - i\omega t}, \tag{B1a}$$

$$\mathbf{E}^{\text{r}} = (E_y^{\text{r}} \mathbf{e}_y + E_{xz}^{\text{r}} (\mathbf{e}_x + \mathbf{e}_z)) e^{i\mathbf{k}'\cdot\mathbf{r} - i\omega t}, \tag{B1b}$$

$$\mathbf{E}^{\text{t}} = (E_y^{\text{t}} \mathbf{e}_y + E_{xz}^{\text{t}} (\mathbf{e}_x - \mathbf{e}_z)) e^{i\mathbf{k}\cdot\mathbf{r} - i\omega t}. \tag{B1c}$$

Here, the wavenumbers are given by $\mathbf{k} = \frac{k}{\sqrt{2}} (\mathbf{e}_x + \mathbf{e}_z)$ and $\mathbf{k}' = \frac{k}{\sqrt{2}} (\mathbf{e}_x - \mathbf{e}_z)$ and the magnitude of the wavenumber k satisfies the dispersion relation $\omega = ck$, where ω is the frequency and c is the light velocity. The corresponding magnetic fields are determined by Faraday's law ($\nabla \times \mathbf{E} = -\partial \mathbf{B} / \partial t$). They read

$$\mathbf{B}^{\text{in}} = \frac{E^{\text{in}}}{\sqrt{2}c} (\mathbf{e}_z - \mathbf{e}_x) e^{i\mathbf{k}\cdot\mathbf{r} - i\omega t}, \tag{B2a}$$

$$\mathbf{B}^{\text{r}} = \frac{1}{\sqrt{2}c} (-2E_{xz}^{\text{r}} \mathbf{e}_y + E_y^{\text{r}} (\mathbf{e}_x + \mathbf{e}_z)) e^{i\mathbf{k}'\cdot\mathbf{r} - i\omega t}, \tag{B2b}$$

$$\mathbf{B}^{\text{t}} = \frac{1}{\sqrt{2}c} (2E_{xz}^{\text{t}} \mathbf{e}_y + E_y^{\text{t}} (\mathbf{e}_z - \mathbf{e}_x)) e^{i\mathbf{k}\cdot\mathbf{r} - i\omega t}. \tag{B2c}$$

Electrons are driven by the electromagnetic wave in the two-dimensional material, and we treat the responses up

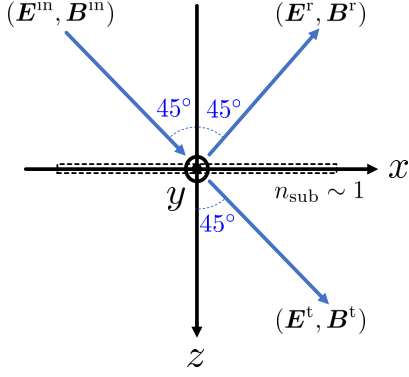


FIG. 6. Schematic diagram visualizing the incident, reflected, and transmitted light beam. The two-dimensional material is put on the xy plane (dashed line).

to the linear order. In the following, we consider that the linear responses only include a usual longitudinal conductivity σ and a magnetoelectric effect χ . These effects appear in a current density as

$$\begin{aligned} j_x &= \sigma_{xx}(\mathbf{E}^t)_x + ik_x\chi(\mathbf{E}^t)_y \\ &= \sigma_{xx}E_{xz}^t + ik_x\chi E_y^t, \end{aligned} \quad (\text{B3})$$

$$\begin{aligned} j_y &= \sigma_{yy}(\mathbf{E}^t)_y - ik_x\chi(\mathbf{E}^t)_x \\ &= \sigma_{yy}E_y^t - ik_x\chi E_{xz}^t. \end{aligned} \quad (\text{B4})$$

This current flows in these two-dimensional metals and influences the boundary conditions of the electromagnetic fields. The boundary conditions coming from Faraday's law and Gauss's law are given by

$$E^{\text{in}} + E_y^{\text{r}} = E_y^{\text{t}}, \quad E_{xz}^{\text{r}} = E_{xz}^{\text{t}}. \quad (\text{B5})$$

Furthermore, Ampère's law gives two boundary conditions as

$$\frac{-1}{\sqrt{2}\mu_0 c}(2E_{xz}^{\text{r}} + 2E_{xz}^{\text{t}}) = \sigma_{xx}E_{xz}^{\text{t}} + i\frac{\omega}{\sqrt{2}c}\chi E_y^{\text{t}}, \quad (\text{B6a})$$

$$\frac{1}{\sqrt{2}\mu_0 c}(E^{\text{in}} - E_y^{\text{r}} - E_y^{\text{t}}) = \sigma_{yy}E_y^{\text{t}} - i\frac{\omega}{\sqrt{2}c}\chi E_{xz}^{\text{t}}. \quad (\text{B6b})$$

Here, μ_0 is the vacuum permeability. Solving these equations simultaneously, we find

$$\frac{E_{xz}^{\text{t}}}{E_y^{\text{t}}} = -\frac{i\omega\chi}{\sqrt{2}c}\left(\frac{2\sqrt{2}}{\mu_0 c} + \sigma_{xx}\right)^{-1} \equiv te^{i\phi_t}, \quad (\text{B7})$$

$$\begin{aligned} \frac{E_{xz}^{\text{r}}}{E_y^{\text{r}}} &= \frac{i\omega\chi}{c(\mu_0 c\sigma_{yy})}\left(\frac{2\sqrt{2}}{\mu_0 c} + \sigma_{xx} - \frac{\omega^2\chi^2}{2c^2\sigma_{yy}}\right)^{-1} \\ &\sim \frac{i\omega\chi}{c(\mu_0 c\sigma_{yy})}\left(\frac{2\sqrt{2}}{\mu_0 c} + \sigma_{xx}\right)^{-1} \equiv re^{i\phi_r}. \end{aligned} \quad (\text{B8})$$

Here, we ignore the square of χ due to its smallness. This ratio gives the Kerr rotation θ and ellipticity ε as

$$\theta^r = \frac{1}{2} \arctan\left(\frac{2r \cos \phi_r}{1 - r^2}\right), \quad (\text{B9a})$$

$$\varepsilon^r = \tan\left\{\frac{1}{2} \arcsin\left(\frac{2r \sin \phi_r}{1 + r^2}\right)\right\}. \quad (\text{B9b})$$

The Kerr rotation and ellipticity of the transmitted light are obtained by simply replacing r with t .

-
- [1] L. D. Barron, *Molecular Light Scattering and Optical Activity*, 2nd ed. (Cambridge University Press, 2004).
- [2] L. D. Landau, J. S. Bell, M. Kearsley, L. Pitaevskii, E. Lifshitz, and J. Sykes, *Electrodynamics of Continuous Media*, Vol. 8 (Elsevier, 2013).
- [3] R. Pisarev, B. Krichevstov, and V. Pavlov, Optical study of the antiferromagnetic-paramagnetic phase transition in chromium oxide cr2o3, *Phase Transitions: A Multinational Journal* **37**, 63 (1991).
- [4] B. Krichevstov, V. Pavlov, R. Pisarev, and V. Gridnev, Spontaneous non-reciprocal reflection of light from antiferromagnetic cr2o3, *Journal of Physics: Condensed Matter* **5**, 8233 (1993).
- [5] G. Rikken and E. Raupach, Observation of magnetochiral dichroism, *Nature* **390**, 493 (1997).
- [6] T. Arima, Magneto-electric optics in non-centrosymmetric ferromagnets, *Journal of Physics: Condensed Matter* **20**, 434211 (2008).
- [7] M. Fiebig, Revival of the magnetoelectric effect, *Journal of physics D: applied physics* **38**, R123 (2005).
- [8] A. Pimenov, A. Mukhin, V. Y. Ivanov, V. Travkin, A. Balbashov, and A. Loidl, Possible evidence for electromagnons in multiferroic manganites, *Nature physics* **2**, 97 (2006).
- [9] A. B. Sushkov, R. V. Aguilar, S. Park, S.-W. Cheong, and H. D. Drew, Electromagnons in multiferroic ymn₂o₅ and tbmn₂o₅, *Phys. Rev. Lett.* **98**, 027202 (2007).
- [10] H. Katsura, A. V. Balatsky, and N. Nagaosa, Dynamical magnetoelectric coupling in helical magnets, *Phys. Rev. Lett.* **98**, 027203 (2007).
- [11] N. Kida, D. Okuyama, S. Ishiwata, Y. Taguchi, R. Shimano, K. Iwasa, T. Arima, and Y. Tokura, Electric-dipole-active magnetic resonance in the conical-spin magnet ba₂mg₂fe₁₂o₂₂, *Phys. Rev. B* **80**, 220406 (2009).
- [12] I. Kézsmárki, N. Kida, H. Murakawa, S. Bordács, Y. Onose, and Y. Tokura, Enhanced directional dichroism of terahertz light in resonance with magnetic excitations of the multiferroic ba₂coge₂o₇ oxide compound, *Phys. Rev. Lett.* **106**, 057403 (2011).
- [13] Y. Takahashi, R. Shimano, Y. Kaneko, H. Murakawa,

- and Y. Tokura, Magnetolectric resonance with electro-magnons in a perovskite helimagnet, *Nature Physics* **8**, 121 (2012).
- [14] K. Kimura, T. Katsuyoshi, Y. Sawada, S. Kimura, and T. Kimura, Imaging switchable magnetolectric quadrupole domains via nonreciprocal linear dichroism, *Communications Materials* **1**, 39 (2020).
- [15] T. Sato, N. Abe, Y. Tokunaga, and T.-h. Arima, Antiferromagnetic domain wall dynamics in magnetolectric MnTiO_3 studied by optical imaging, *Phys. Rev. B* **105**, 094417 (2022).
- [16] T. Hayashida, K. Arakawa, T. Oshima, K. Kimura, and T. Kimura, Observation of antiferromagnetic domains in Cr_2O_3 using nonreciprocal optical effects, *Phys. Rev. Res.* **4**, 043063 (2022).
- [17] K. Arakawa, T. Hayashida, K. Kimura, R. Misawa, T. Nagai, T. Miyamoto, H. Okamoto, F. Iga, and T. Kimura, Detecting magnetolectric effect in a metallic antiferromagnet via nonreciprocal rotation of reflected light, *Phys. Rev. Lett.* **131**, 236702 (2023).
- [18] K. Natori, Band theory of the optical activity of crystals, *Journal of the Physical Society of Japan* **39**, 1013 (1975).
- [19] H. Zhong, Z. H. Levine, D. C. Allan, and J. W. Wilkins, Band-theoretic calculations of the optical-activity tensor of α -quartz and trigonal se, *Phys. Rev. B* **48**, 1384 (1993).
- [20] V. P. Mineev and Y. Yoshioka, Optical activity of non-centrosymmetric metals, *Phys. Rev. B* **81**, 094525 (2010).
- [21] A. Malashevich and I. Souza, Band theory of spatial dispersion in magnetolectrics, *Phys. Rev. B* **82**, 245118 (2010).
- [22] V. P. Mineev, Magnetostatics and optics of noncentrosymmetric metals, *Phys. Rev. B* **88**, 134514 (2013).
- [23] S. Zhong, J. E. Moore, and I. Souza, Gyrotropic magnetic effect and the magnetic moment on the fermi surface, *Phys. Rev. Lett.* **116**, 077201 (2016).
- [24] J. Ma and D. A. Pesin, Chiral magnetic effect and natural optical activity in metals with or without weyl points, *Phys. Rev. B* **92**, 235205 (2015).
- [25] Y. Gao and D. Xiao, Nonreciprocal directional dichroism induced by the quantum metric dipole, *Phys. Rev. Lett.* **122**, 227402 (2019).
- [26] A. H. Duff and J. E. Sipe, Magnetolectric polarizability and optical activity: Spin and frequency dependence, *Phys. Rev. B* **106**, 085413 (2022).
- [27] Óscar Pozo Ocaña and I. Souza, Multipole theory of optical spatial dispersion in crystals, *SciPost Phys.* **14**, 118 (2023).
- [28] F. Hidalgo, A. Sánchez-Castillo, and C. Noguez, Efficient first-principles method for calculating the circular dichroism of nanostructures, *Phys. Rev. B* **79**, 075438 (2009).
- [29] S. S. Tsirkin, P. A. Puente, and I. Souza, Gyrotropic effects in trigonal tellurium studied from first principles, *Phys. Rev. B* **97**, 035158 (2018).
- [30] M. Rérat and B. Kirtman, First-principles calculation of the optical rotatory power of periodic systems: Application on α -quartz, tartaric acid crystal, and chiral (n, m)-carbon nanotubes, *Journal of Chemical Theory and Computation* **17**, 4063 (2021).
- [31] X. Wang and Y. Yan, Optical activity of solids from first principles, *Phys. Rev. B* **107**, 045201 (2023).
- [32] E. S. Morell, L. Chico, and L. Brey, Twisting dirac fermions: circular dichroism in bilayer graphene, *2D Materials* **4**, 035015 (2017).
- [33] T. Stauber, T. Low, and G. Gómez-Santos, Chiral response of twisted bilayer graphene, *Phys. Rev. Lett.* **120**, 046801 (2018).
- [34] K. Chang, Z. Zheng, J. E. Sipe, and J. L. Cheng, Theory of optical activity in doped systems with application to twisted bilayer graphene, *Phys. Rev. B* **106**, 245405 (2022).
- [35] S. T. Ho and V. N. Do, Optical activity and transport in twisted bilayer graphene: Spatial dispersion effects, *Phys. Rev. B* **107**, 195141 (2023).
- [36] J. Ahn, S.-Y. Xu, and A. Vishwanath, Theory of optical axion electrodynamics and application to the kerr effect in topological antiferromagnets, *Nature Communications* **13**, 7615 (2022).
- [37] S. Sekh and I. Mandal, Circular dichroism as a probe for topology in three-dimensional semimetals, *Phys. Rev. B* **105**, 235403 (2022).
- [38] I. Mandal, Signatures of two-and three-dimensional semimetals from circular dichroism, *International Journal of Modern Physics B*, 2450216 (2023).
- [39] J. Ahn and B. Ghosh, Topological circular dichroism in chiral multifold semimetals, *Phys. Rev. Lett.* **131**, 116603 (2023).
- [40] K. Shinada and R. Peters, Unique properties of the optical activity in noncentrosymmetric superconductors: Sum rule, missing area, and relation with the superconducting edelstein effect, *Phys. Rev. B* **108**, 165119 (2023).
- [41] K. Shinada, A. Kofuji, and R. Peters, Quantum theory of the intrinsic orbital magnetolectric effect in itinerant electron systems at finite temperatures, *Phys. Rev. B* **107**, 094106 (2023).
- [42] K. Shinada and R. Peters, Orbital gravitomagnetolectric response and orbital magnetic quadrupole moment correction, *Phys. Rev. B* **107**, 214109 (2023).
- [43] K. Fukushima, D. E. Kharzeev, and H. J. Warringa, Chiral magnetic effect, *Phys. Rev. D* **78**, 074033 (2008).
- [44] M. Tinkham, *Introduction to Superconductivity* (Courier Corporation, 2004).
- [45] H. Watanabe, A. Daido, and Y. Yanase, Nonreciprocal optical response in parity-breaking superconductors, *Phys. Rev. B* **105**, 024308 (2022).
- [46] H. Watanabe, A. Daido, and Y. Yanase, Nonreciprocal meissner response in parity-mixed superconductors, *Phys. Rev. B* **105**, L100504 (2022).
- [47] R. M. Hornreich and S. Shtrikman, Theory of gyrotropic birefringence, *Phys. Rev.* **171**, 1065 (1968).
- [48] L. S. Levitov, Y. V. Nazarov, and G. M. Eliashberg, Magnetolectric effects in conductors with mirror isomer symmetry, *Soviet Physics JETP* **61**, 133 (1985).
- [49] V. M. Edelstein, Magnetolectric effect in polar superconductors, *Phys. Rev. Lett.* **75**, 2004 (1995).
- [50] L. P. Gor'kov and E. I. Rashba, Superconducting 2d system with lifted spin degeneracy: Mixed singlet-triplet state, *Phys. Rev. Lett.* **87**, 037004 (2001).
- [51] S. K. Yip, Two-dimensional superconductivity with strong spin-orbit interaction, *Phys. Rev. B* **65**, 144508 (2002).
- [52] S. Fujimoto, Magnetolectric effects in heavy-fermion superconductors without inversion symmetry, *Phys. Rev. B* **72**, 024515 (2005).
- [53] C.-K. Lu and S. Yip, Signature of superconducting states in cubic crystal without inversion symmetry, *Phys. Rev. B* **77**, 054515 (2008).
- [54] W.-Y. He and K. T. Law, Superconducting orbital

- magnetoelectric effect and its evolution across the superconductor-normal metal phase transition, *Phys. Rev. Res.* **3**, L032012 (2021).
- [55] T. Cheiwchanchamnangij and W. R. L. Lambrecht, Quasiparticle band structure calculation of monolayer, bilayer, and bulk mos_2 , *Phys. Rev. B* **85**, 205302 (2012).
- [56] E. S. Kadantsev and P. Hawrylak, Electronic structure of a single mos_2 monolayer, *Solid State Communications* **152**, 909 (2012).
- [57] W.-Y. He and K. T. Law, Magnetoelectric effects in gyrotropic superconductors, *Phys. Rev. Res.* **2**, 012073 (2020).
- [58] C.-J. Kim, A. Sánchez-Castillo, Z. Ziegler, Y. Ogawa, C. Noguez, and J. Park, Chiral atomically thin films, *Nature nanotechnology* **11**, 520 (2016).
- [59] D. Xiao, W. Yao, and Q. Niu, Valley-contrasting physics in graphene: Magnetic moment and topological transport, *Phys. Rev. Lett.* **99**, 236809 (2007).
- [60] I. Sodemann and L. Fu, Quantum nonlinear hall effect induced by berry curvature dipole in time-reversal invariant materials, *Phys. Rev. Lett.* **115**, 216806 (2015).
- [61] J. Son, K.-H. Kim, Y. H. Ahn, H.-W. Lee, and J. Lee, Strain engineering of the berry curvature dipole and valley magnetization in monolayer mos_2 , *Phys. Rev. Lett.* **123**, 036806 (2019).
- [62] J. Lee, Z. Wang, H. Xie, K. F. Mak, and J. Shan, Valley magnetoelectricity in single-layer mos_2 , *Nature materials* **16**, 887 (2017).
- [63] B. Radisavljevic and A. Kis, Mobility engineering and a metal-insulator transition in monolayer mos_2 , *Nature materials* **12**, 815 (2013).
- [64] J. Ma, K. Deng, L. Zheng, S. Wu, Z. Liu, S. Zhou, and D. Sun, Experimental progress on layered topological semimetals, *2D Materials* **6**, 032001 (2019).
- [65] H. Polshyn, M. Yankowitz, S. Chen, Y. Zhang, K. Watanabe, T. Taniguchi, C. R. Dean, and A. F. Young, Large linear-in-temperature resistivity in twisted bilayer graphene, *Nature Physics* **15**, 1011 (2019).
- [66] X. Lu, P. Stepanov, W. Yang, M. Xie, M. A. Aamir, I. Das, C. Urgell, K. Watanabe, T. Taniguchi, G. Zhang, *et al.*, Superconductors, orbital magnets and correlated states in magic-angle bilayer graphene, *Nature* **574**, 653 (2019).
- [67] N. Kopnin, *Theory of Nonequilibrium Superconductivity* (Oxford University Press, 2001).
- [68] R. A. Ferrell and R. E. Glover, Conductivity of superconducting films: A sum rule, *Phys. Rev.* **109**, 1398 (1958).
- [69] M. Tinkham and R. A. Ferrell, Determination of the superconducting skin depth from the energy gap and sum rule, *Phys. Rev. Lett.* **2**, 331 (1959).
- [70] J. Xia, Y. Maeno, P. T. Beyersdorf, M. M. Fejer, and A. Kapitulnik, High resolution polar kerr effect measurements of sr_2ruo_4 : Evidence for broken time-reversal symmetry in the superconducting state, *Phys. Rev. Lett.* **97**, 167002 (2006).
- [71] A. Kapitulnik, J. Xia, E. Schemm, and A. Palevski, Polar kerr effect as probe for time-reversal symmetry breaking in unconventional superconductors, *New Journal of Physics* **11**, 055060 (2009).
- [72] Z. Tagay, R. Romero III, and N. Armitage, High-precision measurements of terahertz polarization states with a fiber coupled time-domain thz spectrometer, *arXiv preprint arXiv:2312.13276* (2023).
- [73] R. Matsunaga, Y. I. Hamada, K. Makise, Y. Uzawa, H. Terai, Z. Wang, and R. Shimano, Higgs amplitude mode in the bcs superconductors $\text{nb}_{1-x}\text{ti}_x\text{N}$ induced by terahertz pulse excitation, *Phys. Rev. Lett.* **111**, 057002 (2013).
- [74] R. E. Raab and O. L. de Lange, *Multipole Theory in Electromagnetism: Classical, Quantum, and Symmetry Aspects, with Applications* (Oxford University Press, 2004).
- [75] M. Smidman, M. Salamon, H. Yuan, and D. Agterberg, Superconductivity and spin-orbit coupling in non-centrosymmetric materials: a review, *Reports on Progress in Physics* **80**, 036501 (2017).